Geometric method to determine planar anchoring strength for chromonics

Silvia Paparini [*] and Epifanio G. Virga [†]
Department of Mathematics, University of Pavia, Via Ferrata 5, 27100 Pavia, Italy

(Received 29 June 2023; accepted 29 November 2023; published 27 December 2023)

Chromonic nematics are lyotropic liquid crystals that have already been known for half a century, but have only recently raised interest for their potential applications in life sciences. Determining elastic constants and anchoring strengths for rigid substrates has thus become a priority in the characterization of these materials. Here we present a method to determine chromonics' planar anchoring strength. We call it *geometric* as it is based on recognition and fitting of the stable equilibrium shapes of droplets surrounded by the isotropic phase in a thin cell with plates enforcing parallel alignments of the nematic director. We apply our method to shapes observed in experiments; they resemble elongated rods with round ends, which are called *bâtonnets*. Our theory also predicts other droplets' equilibrium shapes, which are either slender and round, called *discoids*, or slender and pointed, called *tactoids*. In particular, sufficiently small droplets are expected to display shape bistability, with two equilibrium shapes, one tactoid and one discoid, exchanging roles as stable and metastable shapes upon varying their common area.

DOI: 10.1103/PhysRevE.108.064701

I. INTRODUCTION

Liquid crystals come in two fashions: Thermotropic and lyotropic. The former are condensed by reducing temperature, the latter by increasing concentration. Chromonic liquid crystals (CLCs) are lyotropic; they are formed by certain dyes, drugs, and nucleic acids. When added to water, these microscopic compounds assemble into *stacks* of molecules, giving rise to rodlike structures that constitute the anisotropic components of the material. At appropriate temperatures and concentrations, these constituents form a nematic phase, which possesses only orientational order, or a more complex columnar phase, which also exhibits a certain degree of positional order [1–5]. Here we shall be concerned with only the nematic phase of CLCs.

Recent times have seen a surge of interest in these phases, mainly because they are soluble in water and so promise to have valuable applications in life sciences [6]. Indeed, success has already been granted to the use of CLCs to detect the presence of toxins and cancer biomarkes in simple devices [7–9].

These and other applications rely on a proper characterization of CLCs, including the determination of elastic constants and anchoring strength on rigid substrates. Here we are especially interested in the latter. We shall propose a method to determine the strength of planar anchoring for chromonics; we call it *geometric*, as it is based on shape recognition and fitting.

The primary motivation for our study came from the experiment performed in [10] on two-dimensional bipolar droplets of chromonic liquid crystals (CLCs) in the nematic phase at equilibrium with their isotropic phase, placed between two parallel plates inducing uniform director alignment. The bounding plates were patterned with submicron-scale linear channels (equally aligned on both plates).

At sufficiently low CLC concentrations, the surface pattern resulted in a preferential alignment of the supramolecular stacks constituting the material with their axes along the surface channels. For large enough concentrations, however, the preferential alignment was still seen to lie on the bounding plates, but at right angles with the surface channels, a phenomenon confirmed and further analyzed in [11]. Here we shall focus attention on the concentration regime for which channels tend to align stacks along their axis. Substrates with this property will be called *aligning*.

Experiments showed essentially *two-dimensional* droplets bearing a *bipolar* director field $\boldsymbol{n}$ with only in-plane components. It is precisely the stable equilibrium shape of these droplets that will be used to determine the anchoring strength of the bounding plates.

The paper is organized as follows. In Sec. II we extend the model employed in [12] for *degenerate* substrates, that is, substrates for which no easy axis is prescribed on the bounding plates. Our analysis will build on our previous work, but we shall thrive to present it in a self-contained manner, leaving out only details that can be easily retrieved. In Sec. III we present our method and apply it to an exemplary case taken from [10]. Special care is given in Sec. III A to make sure that the droplets under study are neither too small nor too large to question the tangential anchoring of the nematic director at their isotropic interface, which is a prerequisite of our analysis. Section IV is devoted to illuminate a typical bistability phenomenon, which we predict to occur for sufficiently small droplets: two different types of shapes coexist at equilibrium, one stable and the other metastable, exchanging their roles at a critical value of the area. Finally, in Sec. V we collect

[*] silvia.paparini@unipv.it
[†] eg.virga@unipv.it

the conclusions of this study. Two Appendixes contain further mathematical details needed to justify a few key passages in our development.

II. FREE BOUNDARY PROBLEM

In this section we present our mathematical theory focused on solving a free boundary problem within a specific class of shapes and director fields.

A. Energetics

We shall denote by $\boldsymbol{n}$ the director field, which represents on a macroscopic scale the average orientation in space of the supramolecular stacks that constitute a CLC. A solid body of experimental evidence (see, for example, [13–15]) suggests that the ground state of CLCs is *not* the one with $\boldsymbol{n}$ uniform in space, as customary in ordinary nematics, but a distorted one, often characterized as a *double twist*.

To appreciate this better, we recall that according to the decomposition of $\nabla\boldsymbol{n}$ proposed by [16] and reprised and reinterpreted by [17] we can write

$$\nabla\boldsymbol{n} = -\boldsymbol{b}\otimes\boldsymbol{n} + \tfrac{1}{2}T\mathbf{W}(\boldsymbol{n}) + \tfrac{1}{2}S\mathbf{P}(\boldsymbol{n}) + \mathbf{D}, \tag{1}$$

where $S := \operatorname{div}\boldsymbol{n}$ is the *splay*, $T := \boldsymbol{n}\cdot\operatorname{curl}\boldsymbol{n}$ is the *twist*, $\boldsymbol{b} := \boldsymbol{n}\times\operatorname{curl}\boldsymbol{n}$ is the *bend*, $\mathbf{W}(\boldsymbol{n})$ is the skew-symmetric tensor associated with the axial vector $\boldsymbol{n}$, $\mathbf{P}(\boldsymbol{n}) : \mathbf{I} - \boldsymbol{n}\otimes\boldsymbol{n}$ is the projection onto the plane orthogonal to $\boldsymbol{n}$, and $\mathbf{D}$ is a symmetric traceless tensor such that $\mathbf{D}\boldsymbol{n} = \mathbf{0}$, which can be represented as

$$\mathbf{D} = q(\boldsymbol{n}_1\otimes\boldsymbol{n}_1 - \boldsymbol{n}_2\otimes\boldsymbol{n}_2). \tag{2}$$

In (2), $(\boldsymbol{n}_1, \boldsymbol{n}_2)$ is an orthonormal pair in the plane orthogonal to $\boldsymbol{n}$ and $q \geqq 0$ is a scalar measure of distortion that we call *octupolar splay* [18]. The bend vector $\boldsymbol{b}$ can be decomposed in the frame $(\boldsymbol{n}_1, \boldsymbol{n}_2, \boldsymbol{n})$ as $\boldsymbol{b} = b_1\boldsymbol{n}_1 + b_2\boldsymbol{n}_2$. We call the scalars (S, T, b_1, b_2, q) distortion *characteristics* of a director field $\boldsymbol{n}$.

A *single* twist is a state of distortion for which $T = \pm 2q$, with q constant and all other distortion characteristics zero; this is, for example, the ground state of cholesterics [19]. On the other hand, a *double* twist is a state of distortion for which T is the only constant distortion characteristic that does not vanish. What distinguishes a double twist from a single twist is that the latter can fill three-dimensional space, whereas the former cannot [20]. Thus, a double twist in the ground state turns necessarily into a source of *frustration*, as it can be achieved locally, but not globally.

The appropriate form of the elastic free energy for CLCs has lately become a matter of debate. The classical Oseen-Frank form W_{OF}, written as [17]

$$W_{\mathrm{OF}} = \tfrac{1}{2}(K_{11} - K_{24})S^2 + \tfrac{1}{2}(K_{22} - K_{24})T^2 + \tfrac{1}{2}K_{33}B^2 + 2K_{24}q^2, \tag{3}$$

where $B^2 := \boldsymbol{b}\cdot\boldsymbol{b}$ and K_{11}, K_{22}, K_{33}, and K_{24} are the *splay*, *twist*, *bend*, and *saddle-splay* constants, has been employed with

$$K_{24} > K_{22}, \tag{4}$$

which aims at making a double twist distortion energetically preferred to no distortion, in violation of Ericksen's inequalities [21]. These inequalities, which are immediately read off from (3), would instead ensure that W_{OF} is positive semidefinite: They are

$$K_{11} \geqq K_{24} \geqq 0, \quad K_{22} \geqq K_{24} \geqq 0, \quad \text{and} \quad K_{33} \geqq 0. \tag{5}$$

It has, however, been shown in [22] that paradoxical consequences follow from (4) for the equilibrium shape of CLC droplets surrounded in three space dimensions by an isotropic fluid, although for fixed domains a variational theory based on (3) could be viable [23]. Other perplexing consequences of (4) were also found for fixed domains in [24].

To remedy such a state of affairs and have a theory that could be applied to fixed and variable domains alike, we proposed in [25] a quartic twist elastic theory based on a density W_{Q} that differs from W_{OF} by a single term proportional to T^4. Further consequences of this theory were also examined in [26].

Here we do not delve any longer on this possibly controversial issue, as in the setting to which our theory will be applied the director field $\boldsymbol{n}$ is *planar*, that is, it lies everywhere parallel to a given plane and is independent of the coordinate orthogonal to that plane. For such a field (see also [27]),

$$T = 0 \quad \text{and} \quad S^2 = 4q^2, \tag{6}$$

and so *both* W_{OF} and W_{Q} reduce to

$$W = \tfrac{1}{2}K_{11}S^2 + \tfrac{1}{2}K_{33}B^2, \tag{7}$$

which is a well-behaved positive-definite energy density for

$$K_{11} > 0 \quad \text{and} \quad K_{33} > 0, \tag{8}$$

the only inequalities needed below.

Where a CLC is in contact with its coexistent isotropic phase, an anisotropic surface tension is present along the interface, which we shall represent by the classical Rapini-Papoular formula [28],

$$W_{\mathrm{s}} = \gamma[1 + \omega(\boldsymbol{n}\cdot\boldsymbol{\nu})^2], \tag{9}$$

where $\gamma > 0$ is the isotropic component of the surface tension at the interface, $\omega > -1$ is a dimensionless parameter weighting the anisotropic component, and $\boldsymbol{\nu}$ is a unit normal to the interface. Here ω is assumed to be positive, so that the interfacial energy density (per unit area) W_{s} is minimized when $\boldsymbol{n}$ is tangent to the interface. Where a CLC is in contact with an aligning substrate, the anchoring energy density W_{a} is represented similarly to (9) as

$$W_{\mathrm{a}} = \tfrac{1}{2}\sigma_0[1 - (\boldsymbol{n}\cdot\boldsymbol{e})^2], \tag{10}$$

where $\sigma_0 > 0$ is the *anchoring strength* and $\boldsymbol{e}$ is a unit vector designating the *easy* axis. In (10), W_{a} is normalized so as to have zero minimum.

B. 2D variational problem

Our theory aims to explain the experiment conducted in [10], which involved coexisting nematic and isotropic phases of a CLC confined within two parallel plates, both treated so

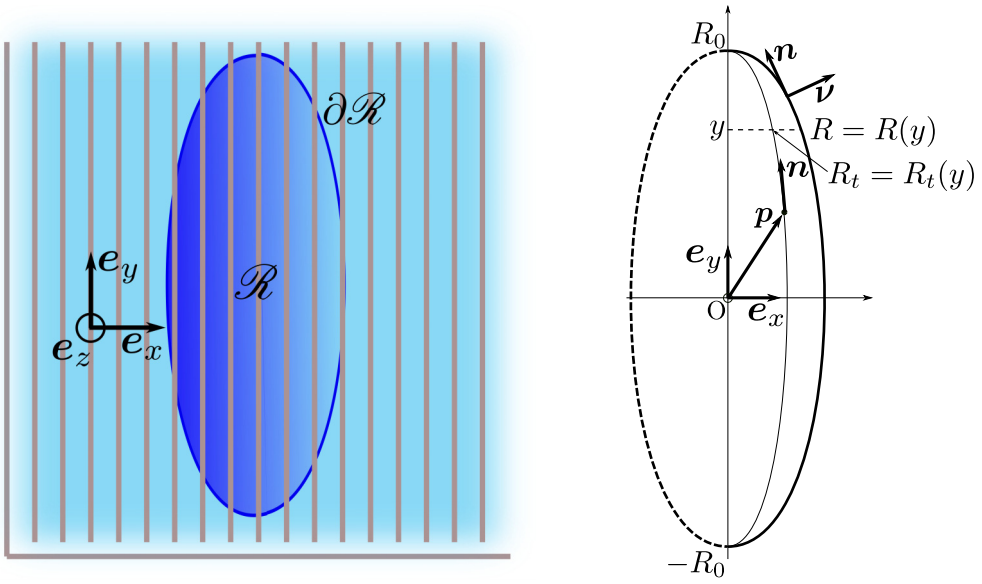

(a) The region $\mathscr{R}$ superimposed to the (schematic) orienting submicron channels.

(b) The boundary $\partial\mathscr{R}$ of $\mathscr{R}$ with outer unit normal $\boldsymbol{\nu}$.

FIG. 1. Two-dimensional problem designed to reproduce the experimental setting of [10]. A CLC island $\mathscr{B}$ surrounded by the isotropic phase is squeezed between two parallel plates patterned with submicron line channels oriented along $\boldsymbol{e}_y$. The cross section $\mathscr{R}$ of the island has area A_0 and it is taken to be mirror symmetric about both x and the y axes. Half of the boundary $\partial\mathscr{R}$ is represented as graph of a smooth, even function $x = R(y)$, where $y \in [-R_0, R_0]$. The bipolar director field $\boldsymbol{n}$ lies on the same plane as $\mathscr{R}$ and is defined as the unit tangent field to the family of curves $x = R_t(y) = g(t)R(y)$, which represent the retractions of $\partial\mathscr{R}$ inside $\mathscr{R}$ for generic $t \in [0, 1]$. Both $\mathscr{R}$ and $\boldsymbol{n}$ should be thought of as uniformly extended through the gap between the parallel plates that bound the cell, at distance h from one another, both orthogonal to the z axis (which comes out of the plane of the figure).

as to induce one and the same parallel uniform easy axis on the nematic phase.[1]

The experimental setting suggests a few assumptions that we shall adopt in our analysis. First, the director field $\boldsymbol{n}$ in the nematic phase is parallel to the bounding plates throughout the cell (and so it is a planar field). Second, each nematic region to which we confine attention will be considered as a cylindrical island $\mathscr{B}$ of prescribed volume V_0 occupying the whole gap between the bounding plates. Third, the cross section $\mathscr{R}$ of $\mathscr{B}$ will be symmetric about the easy axis $\boldsymbol{e}$. We now formulate in a mathematical language these hypotheses.

We take the aligning bounding plates parallel to the (x, y) plane of a Cartesian frame $(\boldsymbol{e}_x, \boldsymbol{e}_y, \boldsymbol{e}_z)$, with $\boldsymbol{e}_y$ coincident with easy axis $\boldsymbol{e}$. We represent the island $\mathscr{B}$ as $\mathscr{R} \times [-\frac{h}{2}, \frac{h}{2}]$, where $\mathscr{R}$ is a region with piecewise smooth boundary $\partial\mathscr{R}$ in the (x, y) plane [see Fig. 1(a)] and h is the cell's thickness. The director field $\boldsymbol{n}$ lies everywhere in the (x, y) plane and is independent of z.

The isoperimetric constraint on the volume of $\mathscr{B}$ translates into a constraint on the area of $\mathscr{R}$,

$$A(\mathscr{R}) = A_0, \tag{11}$$

where A is the area measure and $A_0 = V_0/h$.

[1]Alignment was achieved by use of topographic patterns that had already been characterized for thermotropic liquid crystals [29–31].

With $\omega > 0$ in (9), the interfacial energy density W_s is minimized when $\boldsymbol{n}$ is tangent to $\partial\mathscr{R}$. For simplicity, we shall assume that

$$\boldsymbol{n} \cdot \boldsymbol{\nu} \equiv 0, \quad \text{on} \quad \partial\mathscr{R}, \tag{12}$$

and we shall treat it as a constraint on $\boldsymbol{n}$, save checking its validity *a posteriori* with appropriate energy comparisons (see Sec. III A) to ensure that such a *tangential anchoring* is not broken. In particular, we expect that for aligning substrates assumption (12) may fail to hold for both sufficiently small droplets, as was shown to be the case for degenerate substrates [12], and for sufficiently large droplets, for which the anchoring energy W_a is more likely to prevail over W_s.

Adding all energy contributions discussed above, with the aid of (7), (9), and (10), we arrive at the following total free-energy functional $\mathscr{F}$, which describes a chromonic island $\mathscr{B}$ with cross section $\mathscr{R}$,

$$\begin{aligned}\mathscr{F}[\mathscr{R}; \boldsymbol{n}] &:= h\left\{\frac{1}{2}\int_{\mathscr{R}} [K_{11}(\operatorname{div}\boldsymbol{n})^2 + K_{33}|\boldsymbol{n} \times \operatorname{curl}\boldsymbol{n}|^2]dA + \gamma\,\ell(\partial\mathscr{R})\right\} \\ &\quad - \sigma_0 \int_{\mathscr{R}} (\boldsymbol{n} \cdot \boldsymbol{e}_y)^2 dA,\end{aligned} \tag{13}$$

where $\ell(\partial\mathscr{R})$ denotes the length of $\partial\mathscr{R}$ and use has been made of (12). In (13), an additive constant, $\sigma_0 A_0$, has been omitted; it plays no role in the minimum problem studied here, in force

of the isoperimetric constraint (11), which prescribes the area A_0 of the admissible domains $\mathscr{R}$.

C. Shapes and director fields

The shape of $\mathscr{R}$ is the primary unknown of our minimum problem. Free boundary problems like this are usually very difficult when treated in great generality, even in two space dimensions (as also witnessed by a recent analytic study [32]). Following a well-established tradition (see, for example, the papers [33–39]), we shall tackle this problem in a special class of admissible shapes for $\mathscr{R}$.

Inspired by the experimental setting of [10], we shall assume that the long axis of $\mathscr{R}$ is aligned with $\boldsymbol{e}_y$ and that the shape of $\mathscr{R}$ is mirror symmetric about both the x and the y axes of the frame $(\boldsymbol{e}_x, \boldsymbol{e}_y)$. Thus, only half of the curve that bounds $\mathscr{R}$ needs to be described, the other half being obtained by mirror symmetry. More precisely, $\partial\mathscr{R}$ will be described as the graph of a smooth, even function $x = R(y)$ defined over the interval $[-R_0, R_0]$, which is to be determined. The function R vanishes at the end points of this interval; they designate the *poles* of the drop [see Fig. 1(b)],

$$R(\pm R_0) = 0. \tag{14}$$

Smoothness and symmetry require $R'(0) = 0$, where a prime denotes differentiation with respect to the argument. Whenever $R'(R_0)$ is finite, the surface normal is discontinuous at the poles and the shape $\mathscr{R}$ is a *genuine* tactoid; conversely, when $R'(R_0)$ is unbounded, $\partial\mathscr{R}$ is everywhere smooth.

We shall use the method devised in [12] to obtain a bipolar director field $\boldsymbol{n}$ inside $\mathscr{R}$ from the mere knowledge of $\partial\mathscr{R}$; this consists in retracting $\partial\mathscr{R}$ inside $\mathscr{R}$ to generate a family of nonintersecting curves filling the whole of $\mathscr{R}$ with $\boldsymbol{n}$ everywhere tangent to them. More precisely, $\boldsymbol{n}$ is defined as the unit vector field tangent to the retracting inner curve $R_t(y) := g(t)R(y)$, where $t \in [0, 1]$ and g is an increasing function such that $g(0) = 0$ and $g(1) = 1$. Figure 1(b) illustrates a sketch for such retracting lines; we will find the total free energy to be independent of the specific function g, and so of the specific method of retraction.

We rescale both y and $R(y)$ to the radius R_e of the *equivalent* disk with area A_0, keeping their names unchanged, while we denote by μ the ratio

$$\mu := \frac{R_0}{R_e}. \tag{15}$$

With this normalization, the area constraint (11) reads simply as

$$\int_{-\mu}^{\mu} R(y)dy = \frac{\pi}{2} \tag{16}$$

and (14) becomes

$$R(\pm\mu) = 0. \tag{17}$$

Reasoning as in [12], we can reduce $\mathscr{F}$ in (13) to the following functional in the scaled variables y and $R(y)$:

$$\mathcal{F}[\mu; R] := \frac{\mathscr{F}[\mathscr{R}; \boldsymbol{n}]}{K_{11}h} = \mathcal{F}_e[\mu; R] + \mathcal{F}_a[\mu; R], \tag{18}$$

where

$$\mathcal{F}_e[\mu; R] := \int_{-\mu}^{\mu} \left\{ \left[\frac{R'}{R} - \frac{R''}{R'} + \frac{1}{8}\frac{RR''^2}{R'^3}(3 + k_3) \right] \arctan R' + \frac{R''}{1 + R'^2} + \frac{1}{8}\frac{RR''^2}{(1 + R'^2)^2} \left[(k_3 - 5) - \frac{1}{R'^2}(3 + k_3) \right] + 2\alpha\sqrt{1 + R'^2} \right\} dy \tag{19}$$

is the scaled elastic free energy functional [see Eq. (11) of [12]], while

$$\mathcal{F}_a[\mu; R] := -4\beta\alpha^2 \int_{-\mu}^{\mu} \frac{R}{R'} \arctan R' dy \tag{20}$$

is the appropriate dimensionless form of the anchoring energy for aligning substrates (see Appendix A). In (19),

$$k_3 := \frac{K_{33}}{K_{11}} \tag{21}$$

is the *reduced bend* constant and

$$\alpha := \frac{\gamma R_e}{K_{11}} \tag{22}$$

is a *reduced area*.[2] In (20),

$$\beta := \frac{\sigma_0 K_{11}}{2h\gamma^2} \tag{23}$$

is the *dimensionless anchoring* strength of the substrates.

Both α and β are dimensionless parameters: while α is the ratio of two forces, β does *not* have an equally transparent physical interpretation. The parameter $\widetilde{\beta} := 2\alpha^2\beta = \sigma_0 R_e^2/K_{11}h$ would seem to be more meaningful, as it is the ratio of two energies. As will become clear in Sec. III, in the present setting (for $R_e \sim 10\,\mu$m and $\sigma_0 \sim 10$–$10^2\,\mu\text{Jm}^{-2}$) we expect that $\alpha \sim 10^2$ and $\widetilde{\beta} \sim 10^2$–$10^3$, which makes $\beta \sim 10^{-2}$–10^{-1}. Here to simplify comparison with experiment, we choose to estimate α from other sources and not to use it as an independent fitting parameter. This makes β and $\widetilde{\beta}$ interchangeable. According to (19), the value $k_3 = 5$ seems to be somewhat special: for $k_3 > 5$, two similar terms in the integrand would become antagonistic; we lack an explanation for this, but we heed that $k_3 < 5$ for the material of the experiment in [10] (see Sec. III).

As a consequence of (17), the functional $\mathcal{F}_e$ in (18) diverges logarithmically to $+\infty$ near the poles of $\mathscr{R}$, due to the nonintegrablity at $y = \pm\mu$ of the integrand $\frac{R'}{R}\arctan R'$.[3] The poles of $\mathscr{R}$ are also the points where $\boldsymbol{n}$ exhibits *surface* defects, also known as *boojums*; following a common practice (see, for example, [41], p. 171) we tame these singularities by replacing them with isotropic *cores* of size ε (in R_e units).

[2]Equivalently, $\alpha = R_e/\xi_e$, where ξ_e is the de Gennes-Kleman *extrapolation length* [40, p. 159]. In this language, a drop is either *small* or *large*, whether $\alpha \ll 1$ or $\alpha \gg 1$, respectively.

[3]Despite the apparent similarity between this integrand and that in (20), the latter stays bounded, irrespective of the limiting value of $R'(y)$ for $y \to \pm\mu$ (no matter whether finite or not).

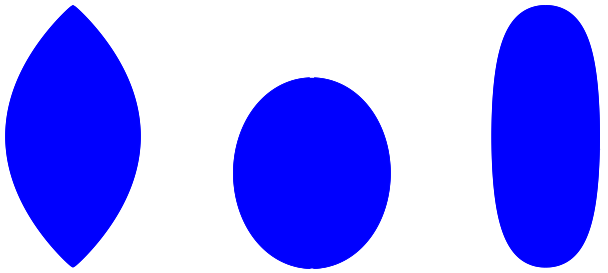

(a) tactoid $\phi = 0.1 \quad \mu = 1.5$ (b) discoid $\phi = 1.6 \quad \mu = 1.1$ (c) bâtonnet $\phi = 1.9 \quad \mu = 1.5$

FIG. 2. Gallery of exemplary shapes with profile as in (25) obtained for different values of parameters (ϕ, μ), each showing a different type of possible convex minimizer of $\mathcal{F}$ in (18). Tactoids *conventionally* occur for $0 \leqq \phi < 0.20$, discoids for $0.20 \leqq \phi < 1.77$, and bâtonnets for $1.77 \leqq \phi < 2.03$. The value of ϕ assigns the type of shape represented by (25), while μ affects its aspect ratio according to (26): for given ϕ, the polar distance grows quadratically with μ relative to the width.

Thus, the integrals in (18) and (19) can be taken over a shorter interval $[-\eta, \eta]$, where η is such that [12]

$$R(\eta) = R(-\eta) = \varepsilon. \tag{24}$$

For R_e in the order of 10 μm, it is reasonable to take $\varepsilon \sim 10^{-3}$. As shown in Appendix B, the extra energy stored in the defect cores does *not* depend on ε and is negligible compared with the surface anchoring energy, so that it plays no role in the global minimum problem.

D. Special family of shapes

Here to simplify the analysis of the functional $\mathcal{F}$ in (18), we represent the admissible shapes of $\mathscr{R}$ by a two-parameter family of functions $R(y)$. Specifically, we let

$$R(\phi, \mu; y) = \frac{\pi}{H(\phi)} \frac{1}{\mu} \left\{ \left[1 - \left(\frac{y}{\mu} \right)^2 \right] \cos\phi + \sqrt{1 - \left(\frac{y}{\mu} \right)^2} \sin\phi \right\},$$

$$\text{with} \quad H(\phi) := \frac{8}{3} \cos\phi + \pi \sin\phi > 0. \tag{25}$$

The parameters (ϕ, μ) describe a two-dimensional configuration space $\mathsf{S} := \{(\phi, \mu) : 0 \leqq \phi \leqq \frac{3\pi}{4}, \mu > 0\}$, where the bounds on ϕ imply that $H > 0$. More details on the geometric construction that justifies (25) can be found in [12]. Here we heed only that while by (17) μ represents the polar distance of $\mathscr{R}$, different values of ϕ affect its shape: conventionally, $\mathscr{R}$ is said to be a *tactoid* for $0 \leqq \phi < \frac{\pi}{16}$, a *discoid* for $\frac{\pi}{16} \leqq \phi < \frac{9\pi}{16}$, and a *bâtonnet*[4] for $\frac{9\pi}{16} \leqq \phi < \phi_c := \operatorname{arccot}(-\frac{1}{2})$. Genuine tactoids occur only for $\phi = 0$. Representatives of these types of admissible shapes are depicted in Fig. 2. They are all convex; nonconvex shapes can also be represented by (25) for $\phi > \phi_c$, but they play no role in our analysis, as they do not minimize $\mathcal{F}$.

Within the class of shapes described by (25), the aspect ratio δ of $\mathscr{R}$ can be expressed as an explicit function of the parameters (ϕ, μ),

$$\delta(\phi, \mu) := \frac{\mu}{R(\phi, \mu; 0)} = \frac{\mu^2 \left(\frac{8}{3} \cos\phi + \pi \sin\phi \right)}{\pi (\cos\phi + \sin\phi)}. \tag{26}$$

The major advantage of using (25) to represent the admissible shapes of $\mathscr{R}$ is that the functional $\mathcal{F}$ in (18) reduces to a function $F(\alpha, \beta; \phi, \mu)$ defined on S for any given value of the pair (α, β). We need only to minimize F over S to obtain an approximate minimizer $\mathscr{R}$ of $\mathscr{F}$, a task that can be accomplished numerically with fairly standard methods.

III. GEOMETRIC METHOD

We wish to apply the theory outlined in Sec. II to interpret the experiment performed in [10]. There two aligning substrates consisting in replicas of 250 nm-deep linear channels equally spaced at 250 nm were overlaid parallel to one another, separated by a gap of 7 μm; the cell they delimited was filled with a DSCG solution prepared at concentration $c = 11$ wt% by dissolving the chromonic material in deionized water. At temperature $T = 25\,^\circ$C, elongated bâtonnets were observed with a dipolar director field $\boldsymbol{n}$ on their boundaries and their long axes aligned to the channels.

In particular, we shall focus on the droplet shown in Fig. 12(a) of [10] (and highlighted in Fig. 3). Its area A_0 and aspect ratio δ are estimated to be

$$A_0 \approx 3217\,\mu\text{m}^2 \quad \text{and} \quad \delta \approx 2.4, \tag{27}$$

the former corresponding to $R_e \approx 32\,\mu$m. We read off from the phase diagram for DSCG in Fig. 2(a) of [42] that at $T = 25\,^\circ$C the concentration of the coexisting nematic phase is approximately 13.5 wt%, larger than the concentration of the preparation (as expected). Using the curves that in [43] represent the temperature dependence of the elastic constants of the nematic phase of DSCG at $c = 14$ wt%, we readily find that at $T = 25\,^\circ$C

$$K_{11} \approx 3\,\text{pN} \quad \text{and} \quad k_3 \approx 4.5. \tag{28}$$

As for the isotropic surface tension γ, we take the estimate $\gamma \approx 10\,\mu\text{J/m}^2$ suggested by our previous study [12]). We then obtain from (28) and (22) that $\alpha \approx 110$.[5]

Some estimates of the anchoring strength σ_0 for chromonics in contact with different substrates are already known: They range from $\sigma_0 \sim 10^{-1}\,\mu\text{J/m}^2$, for both scratched glasses [11] and rubbed polyimide surfaces [44], to $\sigma_0 \sim 10^2\,\mu\text{J/m}^2$, for surfaces lithographed by secondary sputtering [45].[6] In the experiment under consideration, the aligning surfaces

[4]Name borrowed from French, meaning *short staff*.

[5]We are aware that such an estimate for α may be affected by the value chosen for γ, that applies to a DSCG solution in conditions different than the ones occurring in [10]. Unfortunately, we lack better data.

[6]For thermotropic liquid crystals, the strength of planar anchoring ranges from about 1 $\mu\text{J/m}^2$ to one or two orders of magnitude higher, as shown, for example, in Table 3.1 of [46]. On the strongest side

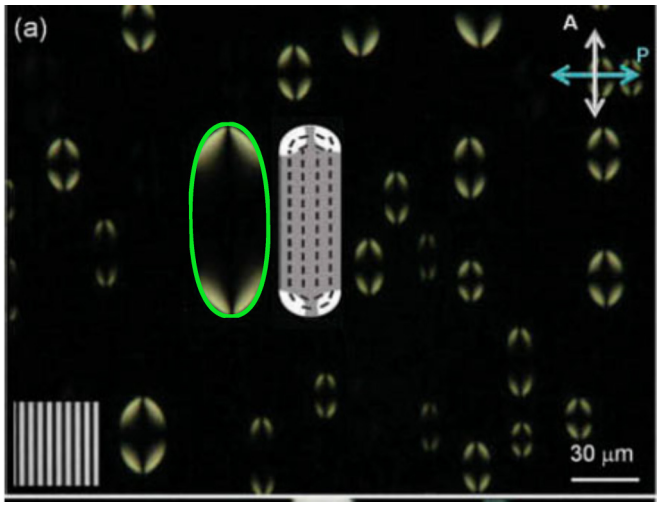

FIG. 3. Experimental picture, borrowed from Fig. 12(a) of [10], representing the top view of a cell of thickness $h = 7\,\mu\text{m}$ filled with DSCG prepared at concentration $c = 11$ wt% and observed between crossed polarizers (marked on the top right corner) in the coexisting biphasic regime (where the concentration of the nematic phase is estimated to be $c \approx 13.5$ wt%). The white stripes on the bottom left corner designate the orientation of the aligning channels on both bounding substrates. The droplet outlined in green corresponds to the minimizer $\phi_0 \doteq 1.77$ and $\mu_0 \doteq 1.51$ of the free energy $F(\alpha, \beta; \phi, \mu)$ for $\alpha = 110$ and $\beta = 5.5 \times 10^{-2}$, the latter identified so as to fit the experimental value $\delta \approx 2.4$ of the droplet's aspect ratio, as shown in Fig. 4. The polar distance is $2R_0 = 2\mu R_e \approx 96\,\mu\text{m}$ (for $R_e \approx 32\,\mu\text{m}$). The green outline, obtained from (25), is superimposed to the experimental image. The whitish cartoon is an illustration (proposed in [10]) of the observed director field; it is not meant to represent closely the droplet's shape.

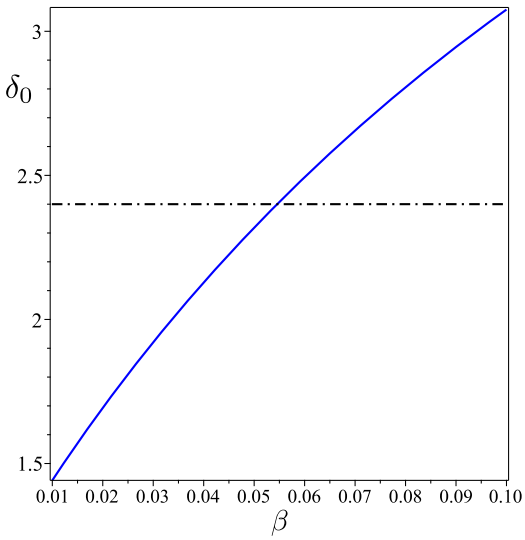

FIG. 4. Graph of the aspect ratio $\delta_0 = \delta(\phi_0, \mu_0)$ according to (26) for the minimizer (ϕ_0, μ_0) of the free energy $F(\alpha, \beta; \phi, \mu)$ for $\alpha = 110$, $k_3 = 4.5$, and $0.01 \leqq \beta \leqq 0.1$.

were lithographed, and so we expect σ_0 to be in the range 10–$10^2\,\mu\text{J/m}^2$. By using $K_{11} \sim 1\,\text{pN}$ from (28) and $\gamma \sim 10\,\mu\text{J/m}^2$ from [12], for $h \sim 10\,\mu\text{m}$, we estimate from (23) that $\beta \sim 10^{-2}$.

We thus seek numerically the minimum of $F(\alpha, \beta; \phi, \mu)$ in the pair (ϕ, μ) for $\alpha = 110$ and $0.01 \leqq \beta \leqq 0.1$; for every value of β in this interval, we compute the theoretical value of the aspect ratio δ according to (26), obtaining the graph shown in Fig. 4.

The experimental value of δ is met for

$$\beta \doteq 5.5 \times 10^{-2} \tag{29}$$

and the corresponding coordinates of the energy minimizer in S are $\phi_0 \doteq 1.77$ and $\mu_0 \doteq 1.51$. The predicted equilibrium shape is a bâtonnet, which is to be compared with the shape of the droplet experimentally observed in Fig. 3. Theory and experiment seem to be in good agreement. By combining (29) and (23), we arrive at the following estimate of the anchoring strength:

$$\sigma_0 \approx 26\,\mu\text{J/m}^2, \tag{30}$$

which turns out to have the same order of magnitude as γ and intermediate between values measured with other methods for the same material.

A. Tangential anchoring breaking

As in our previous work [12], the theory presented here is based on the assumption that the director configuration at the boundary of the drop remains bipolar for all admissible values of the area A_0.

Although the validity of this constraint is confirmed experimentally, we are aware that it cannot hold for all values of A_0, as the tangential anchoring of $\boldsymbol{n}$ is bound to be broken both for A_0 sufficiently small and for A_0 sufficiently large. Indeed, for given h, the elastic, interfacial, and anchoring energies scale like R_e^0, R_e^1, and R_e^2, respectively (see also [49], for a similar reasoning). Thus, for $\alpha \ll 1$, the elastic energy dominates, promoting a uniform orientation of $\boldsymbol{n}$, preferentially along the aligning channels. On the other hand, for $\alpha \gg 1$, the anchoring energy dominates, promoting the same uniform alignment of $\boldsymbol{n}$. In both limiting cases, the tangential anchoring at the isotropic interface is broken.

Direct energy comparisons performed with the method illustrated in Appendix B of [12] (based on constructions by Wulff [50] and Williams [51]) allowed us to estimate an interval $\alpha_1 \leqq \alpha \leqq \alpha_2$, within which we can be confident that the tangential anchoring hypothesized here on the isotropic interface is *not* broken. The end points of such a *safeguard* interval for α were identified as the farthest apart roots of the following polynomial in α as λ ranges in the

is the measurement of [47], based on an improved reflectometric method introduced in [48]; for 5CB, it was found that $\sigma_0 \sim 10^2\,\text{J/m}^2$.

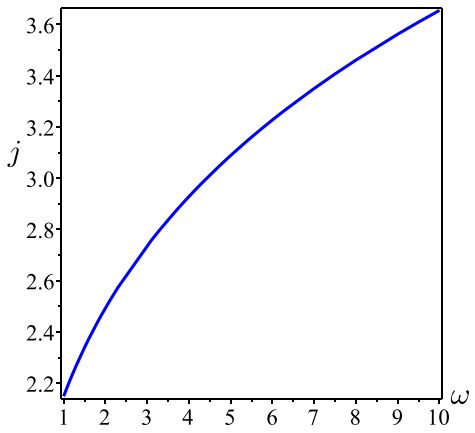

(a) Graph of the function $j(\omega)$ (from Fig. 13b of [12]).

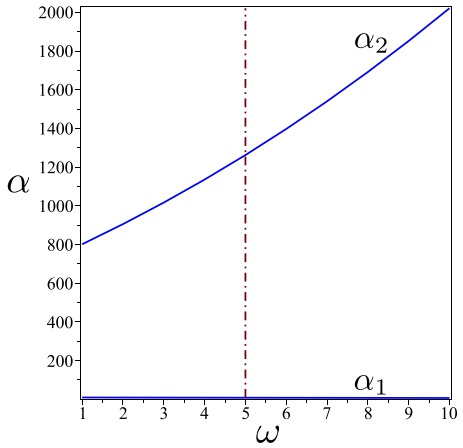

(b) Farthest apart roots of the polynomial P_λ in (31) plotted against ω.

FIG. 5. Roots of polynomial $P_\lambda(\alpha)$ in (31) as λ ranges in the interval (0,1], for $\varepsilon = 10^{-3}$ and β and k_3 as in (29) and (28), respectively.

interval $0 < \lambda \leqq 1$,

$$P_\lambda(\alpha) := -\frac{1}{3}\beta\lambda^2\alpha^2 + \left[4j(\omega) - 4\lambda\left(\frac{\pi}{2} - \varepsilon\right) - \frac{\pi}{\lambda}(1-\lambda^2) - 2\omega\lambda\pi\varepsilon\right]\alpha - 4\left[\frac{\pi}{4}(k_3 - 1 - k_3\ln 2 - \ln\varepsilon) + \varepsilon\right], \tag{31}$$

where j is a monotone function of the dimensionless anisotropic strength ω in (9) [see Fig. 5(a)]. Figure 5(b) shows how both α_1 and α_2 depend on ω (the latter more dramatically than the former) for $\varepsilon = 10^{-3}$ and β and k_3 as in (29) and (28), respectively. Letting $\omega = 5$, which is a choice supported by some evidence [38,52], we obtain that $\alpha_1 \doteq 7$ and $\alpha_2 \doteq 1262$, showing that the case we have studied ($\alpha \approx 110$) falls well inside the range of validity of our model.[7]

In the following section, we shall explore the equilibrium shapes of $\mathscr{R}$ for values of α both smaller and larger than the one corresponding to the experimental shape outlined in Fig. 3, but still within the safeguard interval identified above. We shall see that for sufficiently small droplets our theory also predicts *shape bistability* in the present setting of aligning substrates, as it did in [12] for planar degenerate ones.

IV. SHAPE BISTABILITY

We extended the analysis of the minimizers of the reduced free energy function $F(\alpha, \beta; \phi, \mu)$ by allowing α to cover the whole safeguard interval corresponding to the values of k_3 and β in (28) and (29), respectively. Our aim was to see whether our theory would also predict droplets' equilibrium shapes qualitatively different than those observed in [10] (representative examples of which are reported in Fig. 3). We found out that it *does*, in a range of sufficiently small values of the droplets' area; they do not seem to have been observed, at least in [10].

In brief, we found that, for α in the interval $\alpha_* \leqq \alpha \leqq \alpha^*$, *two* equilibrium shapes compete for the global energy minimizer, a tactoid and a discoid, coexisting as local minimizers and exchanging their role as global minimizer at a critical value, $\alpha = \alpha_b$, of perfect bistability. Details of our analysis are illustrated in the bifurcation diagrams with hysteresis shown in Fig. 6.

For $\alpha < \alpha_*$, only the (blue) tactoidal branch exists and is globally stable. As soon as α exceeds α_* the (red) discoidal branch comes into life as a metastable equilibrium and takes over the tactoidal branch as energy minimizer at $\alpha = \alpha_b$. Two black dots mark the exchange of stability occurring in the system; close to them in Fig. 6(a) are placed the corresponding equilibrium shapes depicted in the same color as the equilibrium branch they belong to. For $\alpha > \alpha_b$, the metastable tactoidal branch ceases altogether to exist at $\alpha = \alpha^*$ and gives way to the discoidal one as unique equilibrium branch. In an interval, the ϕ trajectory of energy minimizers in Fig. 6(a) traverses the bâtonnet border, while staying otherwise in the discoidal territory for $\alpha > \alpha^*$. For $\alpha < \alpha_*$, instead, the ϕ trajectory stays consistently within the tactoidal territory.

Two features deserve notice. First, discoids are energy minimizers, but not for all values of α: upon increasing the droplet's area, the equilibrium shape undergoes two smooth transitions, from a discoid to a bâtonnet and back again to a discoid. Second, as shown by both Figs. 6(b) and 6(c), upon increasing the droplet's area in the whole admissible domain, the equilibrium shape is first thickened and then thinned, suffering a transient setback at the transition.

The transition values of α shown in Fig. 6 are $\alpha_* \approx 60$, $\alpha_b \approx 80$, and $\alpha^* \approx 96$, while the reentrant bâtonnet interval in Fig. 6(a) is $106 \leqq \alpha \leqq 160$, where in particular falls the value $\alpha \approx 110$ corresponding to the droplet outlined in Fig. 3. In physical units, according to the model proposed here, one would then expect coexistence of tactoids and discoids for $18\,\mu\text{m} \lessapprox R_e \lessapprox 29\,\mu\text{m}$, a regime of small droplets for which no data are available in [10]. For $R_e \gtrapprox 29\,\mu\text{m}$, only nontactoidal shapes should be observed; they

[7]Reverting the safeguard interval for α into one for the equivalent radius R_e, we arrive at $0.1\,\mu\text{m} \lessapprox R_e \lessapprox 0.4\,\text{mm}$, confirming again that in the case of interest ($R_e \approx 32\,\mu\text{m}$) our theory is perfectly legitimate.

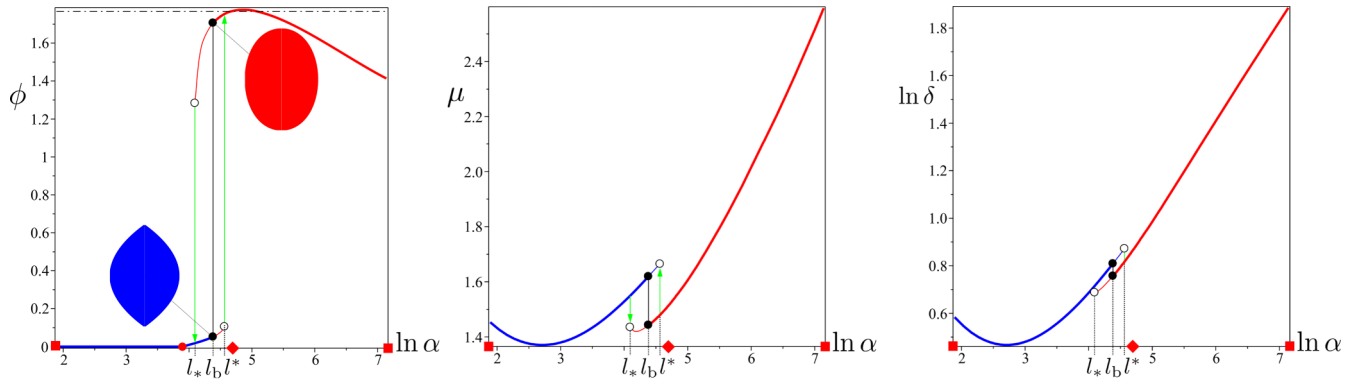

(a) Minimizers' ϕ trajectory (b) Minimizers' μ trajectory (c) Droplet's aspect ratio

FIG. 6. Bifurcation diagrams with hysteresis of the energy minimizers drawn for $k_3 = 4.5$ and $\beta = 5.5 \times 10^{-2}$; thick lines represent global minimizers (stable branches) of $F(\alpha, \beta; \phi, \mu)$ in the pair (ϕ, μ), while thin lines represent local minimizers (metastable branches). Open circles mark the equilibrium shapes that delimit the interval of coexistence of tactoidal and discoidal shapes, while green lines bound the corresponding shape hysteresis. Black dots identify the two perfectly bistable minimizers. The end points α_1 and α_2 of the safeguard interval for α are marked by (red) squares, while the value $\alpha \approx 110$ corresponding to the shape outlined in Fig. 3 is marked by a (red) diamond. In panel (a), a red dot signals the value of α where the trajectory of minimizers leaves the $\phi = 0$ axis and equilibrium tactoids cease to be genuine. The conventional border of bâtonnets is placed at $\phi \doteq 1.77$, while the tactoidal territory is delimited by the conventional border at $\phi \doteq 0.20$. Here $\alpha_* \approx 60$, $\alpha_b \approx 80$, and $\alpha^* \approx 96$; the following abbreviations are used on the horizontal axis: $l_* := \ln\alpha_* \doteq 4.1$, $l_b := \ln\alpha_b \doteq 4.4$, and $l^* := \ln\alpha^* \doteq 4.6$.

are discoids, except for $32\,\mu\text{m} \lessapprox R_e \lessapprox 48\,\mu\text{m}$, where they are bâtonnets.

V. CONCLUSION

We proposed a method to determine the planar anchoring strength σ_0 of a chromonic liquid crystal on a rigid substrate; its distinctive feature is geometric, as it is based on the observation and fitting of the stable equilibrium shapes of droplets in the nematic phase coexisting in a cell with the isotropic phase. Prior knowledge of the surface tension γ of the nematic phase at the isotropic interface is presumed, which can be gained by use of cells with substrates enforcing planar degenerate anchoring [12].

Our study was motivated by the experiment described in [10], where nematic chromonic droplets formed in a thin cell enclosed within parallel planar substrates orienting the director $\boldsymbol{n}$ in one and the same direction. To illustrate our method, we applied it to one of the DSCG droplets shown in [10] and extracted an estimate for σ_0 from its shape. Although this figure for σ_0 is similar to those obtained with other methods, by no means can our estimate be regarded as a *measure* of σ_0, as it lacks the appropriate statistics and, what is perhaps more important, an independent determination of γ.

Opting for importing the value of γ from other sources, we determined β (and thus σ_0) by fitting the aspect ratio of a selected, representative droplet, judging then the agreement between experiment and theory from a qualitative comparison between observed and predicted shapes. This suffices to provide a proof of principle that the proposed method is indeed viable. It can be improved: using α and $\widetilde{\beta} = 2\alpha^2\beta$ as independent parameters, one could determine *both* γ and σ_0 by fitting an observed shape with the family described in (25) by the parameters (ϕ, μ) (possibly through a shape recognition algorithm). The optimal $(\alpha, \widetilde{\beta})$ would then be determined by minimizing the free energy $F(\alpha, \widetilde{\beta}; \phi_0, \mu_0)$ associated with the best shape represented by (ϕ_0, μ_0). Doing this for several droplets (each with its own R_e) would result in several measures of both γ and σ_0.

One method successfully employed so far to measure σ_0 for chromonics uses twist cells with plates promoting planar easy axes at right angles to one another. Measuring the total *twist angle* Ω across the cell (and how it differs from 90°) determines σ_0, once the twist constant K_{22} is known [53]. This method relies on the theory (put forward by McIntyre [54,55]) relating (in closed form) Ω to the maximum and minimum transmitted intensity of light with normal incidence propagating (between crossed polarizers) through the cell. Although this theory has a wider range of validity than Mauguin's *adiabatic limit* [56] (see also [41], p. 268), it makes approximations too. It might thus be valuable to have an alternative, independent method to rely upon.

Our theory was developed having especially chromonic nematics in mind, but nothing prevents one from applying it to thermotropic nematics as well, as in the setting envisioned here no macroscopic differences arise between these materials.

The droplets' shapes observed in [10] mainly resembled elongated rods with rounded ends, which we called bâtonnets. Theory also predicted other stable equilibrium shapes: either slender and round, which we called discoids, or slender and pointed, which we called tactoids. Moreover, in the range of *small* droplets, we found a regime of bistability, where discoids and tactoids coexist as energy minimizers, taking turns in being alternatively stable or metastable. A similar bistability was also predicted for two-dimensional droplets between parallel plates enforcing planar degenerate anchoring [12], but not for fully three-dimensional droplets [57]. Although these two coincidences *cannot* be a proof,[8] we are inclined to

[8]Common wisdom has it that Agatha Christie once said that one coincidence is a coincidence, two coincidences are a clue, three

think that bistability of shape might be a *two-dimensionality* signature.

ACKNOWLEDGMENTS

We are grateful to the reviewers for their constructive criticism that has improved our work.

APPENDIX A: FURTHER MATHEMATICAL DETAILS

This Appendix contains ancillary calculations used to arrive at the dimensionless form of $\mathscr{F}$ in (19) for the retracted bipolar vector field $\boldsymbol{n}$ described in Sec. II C. A fuller account can be found in [12]. The boundary curve $R = R(y)$ is retracted inside $\mathscr{R}$ as the curve

$$\boldsymbol{p}_t(y) := g(t)R(y)\boldsymbol{e}_x + y\boldsymbol{e}_y, \quad -R_0 \leqq y \leqq R_0, \tag{A1}$$

where $t \in [0, 1]$ and g is any strictly increasing function on [0,1] of class $\mathcal{C}^1$ such that $g(0) = 0$ and $g(1) = 1$. In this two-dimensional setting, $\boldsymbol{n}$ is defined as the unit vector field tangent to the lines represented by (A1) at fixed t; by differentiating $\boldsymbol{p}_t$ in (A1) with respect to y, keeping t fixed, we easily obtain that

$$\boldsymbol{n} = \frac{gR'\boldsymbol{e}_x + \boldsymbol{e}_y}{\sqrt{1 + (gR')^2}}, \tag{A2}$$

where a prime denotes differentiation. The element of area dA of $\mathscr{R}$ is given by

$$dA = dtdyg'R\sqrt{1 + (gR')^2}\boldsymbol{e}_x \times \boldsymbol{n} \cdot \boldsymbol{e}_z = g'Rdtdy. \tag{A3}$$

By rescaling all lengths to the radius R_e of the disk of area A_0, we obtain the following dimensionless form of the total anchoring energy in (13):

$$\begin{aligned}\mathcal{F}_{\mathrm{a}}[\mu; R] &:= -\frac{\sigma_0}{K_{11}h}\int_{\mathscr{R}}(\boldsymbol{n}\cdot\boldsymbol{e}_y)^2 dA \\ &= -2\frac{\sigma_0 R_e^2}{K_{11}h}\int_{-\mu}^{\mu} dy \int_0^1 \frac{g'R}{1 + (gR')^2}dt,\end{aligned} \tag{A4}$$

where μ is defined in (15). By use of (22) and (23), we readily give (A4) the form in (20), which is independent of the specific choice of g, provided this is monotonic and obeys the prescribed boundary conditions.

APPENDIX B: BOOJUM'S DEFECT CORE

Here we estimate the energy stored in the defect core of a boojum on the boundary of a two-dimensional droplet. To this end, we apply a simplified version of Ericksen's model [58]. We write the total free energy in the form

$$\mathscr{F}_{\mathrm{c}}[S, \boldsymbol{n}] := h\int_{\mathscr{C}}\left\{\frac{K}{2}(k|\nabla S|^2 + S^2|\nabla \boldsymbol{n}|^2) + \psi(S)\right\}dA, \tag{B1}$$

where S denotes the scalar order parameter and $\boldsymbol{n}$ is the director field, ψ is the *condensation* potential, K in an average elastic constant, and $0 < k < 1$ is a dimensionless parameter. The domain of integration $\mathscr{C}$ is a circular sector of radius $r_{\mathrm{c}} = \varepsilon R_e$ with (inner) *cusp angle* τ, located at each pole of the region $\mathscr{R}$ shown in Fig. 1: $\tau = \pi$ when $\partial\mathscr{R}$ is smooth, that is, for nongenuine tactoids, discoids, and bâtonnets (see Fig. 2), whereas $\tau < \pi$ for *genuine* tactoids. We write the condensation potential ψ in the standard form,

$$\psi(S) = \tfrac{1}{2}aS^2 - \tfrac{1}{3}bS^3 + \tfrac{1}{4}cS^4, \tag{B2}$$

where a depends on temperature T as $a = A(T - T^*)$, A is a positive constant and T^* is the *supercooling* temperature, while both b and c are positive constant independent of temperature.

The representation for $\mathscr{F}_{\mathrm{c}}$ in (B1) is valid under the assumption that S and $\boldsymbol{n}$ are independent of the coordinate z across the cell confining the droplet. For our estimate, we further take $\boldsymbol{n} = \boldsymbol{e}_r$, where $\boldsymbol{e}_r$ is the unit vector field in the plane (x, y) emanating from the pole of $\mathscr{R}$, and we assume that $S = S(r)$, where r is the radial coordinate, subject to the boundary condition

$$S(r_{\mathrm{c}}) = S_0. \tag{B3}$$

Here for $b^2 > 4ac$,

$$S_0 := \frac{b + \sqrt{b^2 - 4ac}}{2c} \tag{B4}$$

is the absolute minimizer of ψ.

Under these assumptions, by scaling lengths to r_{c}, we give $\mathscr{F}_{\mathrm{c}}$ the following dimensionless form:

$$\begin{aligned}\mathcal{F}_{\mathrm{c}}[S] := \frac{1}{Kh}\mathscr{F}_{\mathrm{c}}[S, \boldsymbol{e}_r] = \tau\int_0^1 \Bigg[\frac{1}{2}kS'^2 + \frac{1}{2}\frac{S^2}{\rho^2} \\ + \xi\left(\frac{1}{2}S^2 - \frac{1}{3}b_0S^3 + \frac{1}{4}c_0S^4\right)\Bigg]\rho d\rho,\end{aligned} \tag{B5}$$

where

$$\rho := \frac{r}{r_{\mathrm{c}}}, \quad \xi := \frac{ar_{\mathrm{c}}^2}{K}, \quad b_0 := \frac{b}{a}, \quad c_0 := \frac{c}{a}, \tag{B6}$$

and a prime denotes differentiation with respect to ρ. In (B5), ξ weights the condensation energy against the elastic energy. To estimate this dimensionless parameter, we resort to the classical data of [59] (see also [40], p. 130) and for $T - T^* \sim 1\,\mathrm{K}$, $r_{\mathrm{c}} \sim 10\,\mathrm{nm}$, and $K \sim 1\,\mathrm{pN}$, we find that $\xi \sim 1$.[9] Thus, elastic and condensation components of the free energy in (B5) have the same order of magnitude. Since $\psi(S) \geqq \psi(S_0)$ for $0 \leqq S \leqq S_0$, $\mathcal{F}_{\mathrm{c}}$ satisfies the inequality

$$\begin{aligned}\mathcal{F}_{\mathrm{c}}[S] \geqq \frac{1}{2}\tau\int_0^1\left(kS'^2 + \frac{S^2}{\rho^2}\right)\rho d\rho \\ + \frac{1}{2}\tau\xi S_0^2\left(\frac{1}{2} - \frac{1}{3}b_0S_0 + \frac{1}{4}c_0S_0^2\right).\end{aligned} \tag{B7}$$

coincidences a proof. We could not locate this precise quote in her writings, but in *The ABC Murders* M. Poirot comes close when he says, "It is the same motif three times repeated. That cannot be coincidence."

[9] More precisely, for MBBA, we learn from [59] that $\frac{1}{2}A \approx 5 \times 10^4\,\mathrm{Jm^{-3}K^{-1}}$, $\frac{1}{3}b \approx 2 \times 10^5\,\mathrm{Jm^{-3}}$, $\frac{1}{4}c \approx 3 \times 10^5\,\mathrm{Jm^{-3}}$. Since $S \sim 10^{-1}$, for $T - T^* > 1\,\mathrm{K}$, the order of magnitude of $\psi(S)$ is that of aS^2.

An estimate for the the minimum of $\mathcal{F}_c$ can be obtained by minimizing the integral on the right-hand side of (B7) subject to the boundary conditions

$$S(1) = S_0 \quad \text{and} \quad S(0) = 0, \tag{B8}$$

the former stemming from (B4) and the latter being required for $\mathcal{F}_c$ to be finite. The corresponding equilibrium equation is simply given by

$$k(\rho S')' = \frac{S}{\rho}. \tag{B9}$$

The solution to (B9) and (B8) is

$$S = S_0 \rho^{1/\sqrt{k}}. \tag{B10}$$

We thus conclude that the core energy $\mathcal{F}_c$ can be estimated from the inequality

$$\min \mathcal{F}_c[S] \geqq \tfrac{1}{2}\tau S_0^2\big(\sqrt{k} + \xi + \tfrac{1}{2} - \tfrac{1}{3}b_0 S_0 + \tfrac{1}{4}c_0 S_0^2\big), \tag{B11}$$

which substantiates our claim in Sec. II C to the effect that $\mathcal{F}_c$ does not depend on r_c, but only on S_0 and the cusp angle τ. Moreover, since, by (20), $\mathcal{F}_a \sim \alpha^2\beta\mu \sim 10^2$-$10^3$ and, by (B11), $\mathcal{F}_c \sim 10^{-2}$, it is justified to neglect $\mathcal{F}_c$ in the (dimensionless) total free energy $\mathcal{F}$ in (18).

[1] J. Lydon, Chromonic liquid crystalline phases, Liq. Cryst. **38**, 1663 (2011).

[2] J. Lydon, Chromonics, in *Handbook of Liquid Crystals: Low Molecular Weight Liquid Crystals II*, edited by D. Demus, J. Goodby, G. W. Gray, H.-W. Spiess, and V. Vill (John Wiley & Sons, Weinheim, Germany, 1998), pp. 981–1007.

[3] J. Lydon, Chromonic liquid crystal phases, Curr. Opin. Colloid Interface Sci. **3**, 458 (1998).

[4] J. Lydon, Chromonic review, J. Mater. Chem. **20**, 10071 (2010).

[5] I. Dierking and A. Martins Figueiredo Neto, Novel trends in lyotropic liquid crystals, Crystals **10**, 604 (2020).

[6] H.-S. Park and O. D. Lavrentovich, Lyotropic chromonic liquid crystals: Emerging applications, in *Liquid Crystals Beyond Displays: Chemistry, Physics, and Applications*, edited by Q. Li (John Wiley & Sons, Hoboken, NJ, 2012), pp. 449–448.

[7] S. V. Shiyanovskii, T. Schneider, I. I. Smalyukh, T. Ishikawa, G. D. Niehaus, K. J. Doane, C. J. Woolverton, and O. D. Lavrentovich, Real-time microbe detection based on director distortions around growing immune complexes in lyotropic chromonic liquid crystals, Phys. Rev. E **71**, 020702(R) (2005).

[8] C. J. Woolverton, E. Gustely, L. Li, and O. D. Lavrentovich, Liquid crystal effects on bacterial viability, Liq. Cryst. **32**, 417 (2005).

[9] H. Shaban, L. Mon-Juan, and W. Lee, Label-free detection and spectrometrically quantitative analysis of the cancer biomarker CA125 based on lyotropic chromonic liquid crystal, Biosensors **11**, 271 (2021).

[10] Y. Yi and N. A. Clark, Orientation of chromonic liquid crystals by topographic linear channels: Multi-stable alignment and tactoid structure, Liq. Cryst. **40**, 1736 (2013).

[11] A. Mcguire, Y. Yi, and N. A. Clark, Orthogonal orientation of chromonic liquid crystals by rubbed polyamide films, ChemPhysChem **15**, 1376 (2014).

[12] S. Paparini and E. G. Virga, Shape bistability in 2D chromonic droplets, J. Phys.: Condens. Matter **33**, 495101 (2021).

[13] K. Nayani, R. Chang, J. Fu, P. W. Ellis, A. Fernandez-Nieves, J. O. Park, and M. Srinivasarao, Spontaneous emergence of chirality in achiral lyotropic chromonic liquid crystals confined to cylinders, Nat. Commun. **6**, 8067 (2015).

[14] Z. S. Davidson, L. Kang, J. Jeong, T. Still, P. J. Collings, T. C. Lubensky, and A. G. Yodh, Chiral structures and defects of lyotropic chromonic liquid crystals induced by saddle-splay elasticity, Phys. Rev. E **91**, 050501(R) (2015), see also Erratum [60], https://journals.aps.org/pre/supplemental/10.1103/PhysRevE.91.050501/Supplementary_Info_Planar_Davidson_et_al.pdf.

[15] J. Fu, K. Nayani, J. Park, and M. Srinivasarao, Spontaneous emergence of twist and formation of monodomain in lyotropic chromonic liquid crystals confined to capillaries, NPG Asia Mater. **9**, e393 (2017).

[16] T. Machon and G. P. Alexander, Umbilic lines in orientational order, Phys. Rev. X **6**, 011033 (2016).

[17] J. V. Selinger, Interpretation of saddle-splay and the Oseen-Frank free energy in liquid crystals, Liq. Cryst. Rev. **6**, 129 (2018).

[18] A. Pedrini and E. G. Virga, Liquid crystal distortions revealed by an octupolar tensor, Phys. Rev. E **101**, 012703 (2020).

[19] J. V. Selinger, Director deformations, geometric frustration, and modulated phases in liquid crystals, Annu. Rev. Condens. Matter Phys. **13**, 49 (2022).

[20] E. G. Virga, Uniform distortions and generalized elasticity of liquid crystals, Phys. Rev. E **100**, 052701 (2019).

[21] J. L. Ericksen, Inequalities in liquid crystal theory, Phys. Fluids **9**, 1205 (1966).

[22] S. Paparini and E. G. Virga, Paradoxes for chromonic liquid crystal droplets, Phys. Rev. E **106**, 044703 (2022).

[23] S. Paparini and E. G. Virga, Stability against the odds: The case of chromonic liquid crystals, J. Nonlinear Sci. **32**, 74 (2022).

[24] C. Long and J. V. Selinger, Violation of Ericksen inequalities in lyotropic chromonic liquid crystals, J. Elast. **153**, 599 (2023).

[25] S. Paparini and E. G. Virga, An elastic quartic twist theory for chromonic liquid crystals, J. Elast. (2023).

[26] S. Paparini and E. G. Virga, Spiralling defect cores in chromonic hedgehogs, Liq. Cryst. **50**, 1498 (2023).

[27] A. Pedrini and E. G. Virga, Relieving nematic geometric frustration in the plane, J. Phys. A: Math. Theor. **56**, 265202 (2023).

[28] A. Rapini and M. Papoular, Distorsion d'une lamelle nématique sous champ magnétique conditions d'ancrage aux parois, J. Phys. Colloques **30**, C4-54 (1969)

[29] D. K. Yoon, R. Deb, D. Chen, E. Körblova, R. Shao, K. Ishikawa, N. V. S. Rao, D. M. Walba, I. I. Smalyukh, and N. A. Clark, Organization of the polarization splay modulated smectic liquid crystal phase by topographic confinement, Proc. Natl. Acad. Sci. USA **107**, 21311 (2010).

[30] M.-H. Kim, J.-D. Kim, T. Fukuda, and H. Matsuda, Alignment control of liquid crystals on surface relief gratings, Liq. Cryst. **27**, 1633 (2000).

[31] M. Behdani, S. H. Keshmiri, S. Soria, M. A. Bader, J. Ihlemann, G. Marowsky, and T. Rasing, Alignment of liquid crystals with periodic submicron structures ablated in polymeric and indium tin oxide surfaces, Appl. Phys. Lett. **82**, 2553 (2003).

[32] Z. Geng and F. Lin, The two-dimensional liquid crystal droplet problem with a tangential boundary condition, Arch. Ration. Mech. Anal. **243**, 1181 (2022).

[33] A. V. Kaznacheev, M. M. Bogdanov, and S. A.Taraskin, The nature of prolate shape of tactoids in lyotropic inorganic liquid crystals, J. Exp. Theor. Phys. **95**, 57 (2002).

[34] A. V. Kaznacheev, M. M. Bogdanov, and A. S. Sonin, The influence of anchoring energy on the prolate shape of tactoids in lyotropic inorganic liquid crystals, J. Exp. Theor. Phys. **97**, 1159 (2003).

[35] P. Prinsen and P. van der Schoot, Shape and director-field transformation of tactoids, Phys. Rev. E **68**, 021701 (2003).

[36] P. Prinsen and P. van der Schoot, Parity breaking in nematic tactoids, J. Phys.: Condens. Matter **16**, 8835 (2004).

[37] P. Prinsen and P. van der Schoot, Continuous director-field transformation of nematic tactoids, Eur. Phys. J. E **13**, 35 (2004).

[38] N. Puech, E. Grelet, P. Poulin, C. Blanc, and P. van der Schoot, Nematic droplets in aqueous dispersions of carbon nanotubes, Phys. Rev. E **82**, 020702(R) (2010).

[39] A. A. Verhoeff, I. A. Bakelaar, R. H. J. Otten, P. van der Schoot, and H. N. W. Lekkerkerker, Tactoids of plate-like particles: Size, shape, and director field, Langmuir **27**, 116 (2011).

[40] M. Kleman and O. D. Lavrentovich, *Soft Matter Physics: An Introduction*, Partially Ordered Systems (Springer-Verlag, New York, 2003).

[41] P. G. de Gennes and J. Prost, *The Physics of Liquid Crystals*, 2nd ed., International Series of Monographs on Physics (Clarendon Press, Oxford, 1993), vol. 83.

[42] B. Zhang and H.-S. Kitzerow, Influence of proton and salt concentration on the chromonic liquid crystal phase diagram of disodium cromoglycate solutions: Prospects and limitations of a host for DNA nanostructures, J. Phys. Chem. B **120**, 3250 (2016).

[43] S. Zhou, K. Neupane, Y. A. Nastishin, A. R. Baldwin, S. V. Shiyanovskii, O. D. Lavrentovich, and S. Sprunt, Elasticity, viscosity, and orientational fluctuations of a lyotropic chromonic nematic liquid crystal disodium cromoglycate, Soft Matter **10**, 6571 (2014).

[44] P. J. Collings, P. van der Asdonk, A. Martinez, L. Tortora, and P. H. J. Kouwer, Anchoring strength measurements of a lyotropic chromonic liquid crystal on rubbed polyimide surfaces, Liq. Cryst. **44**, 1165 (2017).

[45] J. Y. Kim, K. Nayani, H. S. Jeong, H.-J. Jeon, H.-W. Yoo, E. H. Lee, J. O. Park, M. Srinivasarao, and H.-T. Jung, Macroscopic alignment of chromonic liquid crystals using patterned substrates, Phys. Chem. Chem. Phys. **18**, 10362 (2016).

[46] L. M. Blinov and V. G. Chigrinov, *Electrooptic Effects in Liquid Crystal Materials*, Partially Ordered Systems (Springer, New York, 1994).

[47] S. Faetti and P. Marianelli, Strong azimuthal anchoring energy at a nematic-polyimide interface, Phys. Rev. E **72**, 051708 (2005).

[48] S. Faetti and G. C. Mutinati, An improved reflectometric method to measure the azimuthal anchoring energy of nematic liquid crystals, Eur. Phys. J. E **10**, 265 (2003).

[49] E. G. Virga, Drops of nematic liquid crystals, Arch. Ration. Mech. Anal. **107**, 371 (1989), reprinted in [61].

[50] G. Wulff, Zur Frage der Geschwindigkeit des Wachsthums und der Auflösung der Kristallflächen, Z. Kristal. Mineral. **34**, 449 (1901).

[51] R. D. Williams, Two transitions in tangentially anchored nematic droplets, J. Phys. A: Math. Gen. **19**, 3211 (1986).

[52] Y.-K. Kim, S. V. Shiyanovskii, and O. D. Lavrentovich, Morphogenesis of defects and tactoids during isotropic-nematic phase transition in self-assembled lyotropic chromonic liquid crystals, J. Phys.: Condens. Matter **25**, 404202 (2013).

[53] C. K. McGinn, L. I. Laderman, N. Zimmermann, H.-S. Kitzerow, and P. J. Collings, Planar anchoring strength and pitch measurements in achiral and chiral chromonic liquid crystals using 90-degree twist cells, Phys. Rev. E **88**, 062513 (2013).

[54] P. McIntyre and A. W. Snyder, Light propagation in twisted anisotropic media: Application to photoreceptors, J. Opt. Soc. Am. **68**, 149 (1978).

[55] P. McIntyre, Transmission of light through a twisted nematic liquid-crystal layer, J. Opt. Soc. Am. **68**, 869 (1978).

[56] C. Mauguin, Sur la repŕsentation géometrique de Poincaré relative aux propriétés optiques des piles de lames, Bull. Soc. Fr. Mineral. **34**, 6 (1911), https://gallica.bnf.fr/ark:/12148/bpt6k1089141/f23.item.

[57] S. Paparini and E. G. Virga, Nematic tactoid population, Phys. Rev. E **103**, 022707 (2021).

[58] J. L. Ericksen, Liquid crystals with variable degree of orientations, Arch. Ration. Mech. Anal. **113**, 97 (1991).

[59] Y. Poggi, J. Filippini, and R. Aleonard, The free energy as a function of the order parameter in nematic liquid crystals, Phys. Lett. A **57**, 53 (1976).

[60] Z. S. Davidson, L. Kang, J. Jeong, T. Still, P. J. Collings, T. C. Lubensky, and A. G. Yodh, Erratum: Chiral structures and defects of lyotropic chromonic liquid crystals induced by saddle-splay elasticity [Phys. Rev. E 91, 050501(R) (2015)], Phys. Rev. E **92**, 019905(E) (2015).

[61] E. G. Virga, Drops of nematic liquid crystals, in *Mechanics and Thermodynamics of Continua*, edited by H. Markovitz, V. J. Mizel, and D. R. Owen (Springer, Berlin, 1991), pp. 211–230.